INSTITUTE OF PHYSICS PUBLISHING SMART MATERIALS AND STRUCTURES
Smart Mater. Struct. **13** (2004) 384–392 PII: S0964-1726(04)75013-2

Modelling of a high performance piezoelectric actuator assembly for active and passive vibration control

J X Gao and L Cheng[1]

Department of Mechanical Engineering, The Hong Kong Polytechnic University, Hung Hom, Hong Kong

E-mail: mmjxgao@polyu.edu.hk and mmlcheng@polyu.edu.hk

Received 14 July 2003, in final form 7 January 2004
Published 18 February 2004
Online at stacks.iop.org/SMS/13/384 (DOI: 10.1088/0964-1726/13/2/017)

Abstract
This paper deals with the design and modelling of a novel actuator assembly, in which two THUNDER actuators are put in a clamshell configuration. A simulation model is proposed to describe the mechanical and electrical properties of the actuator assembly on the basis of parameters that can be measured by experiments. In order to validate the model, a system comprising a flexible cantilever beam connected to an actuator is discussed numerically and experimentally. Results show that the novel actuator configuration and the model developed in this paper work very well in the low frequency range. Meanwhile, it is observed that the dynamics of the actuator has an obvious effect on the response of the whole system near the natural frequencies of the actuator itself. Considering the fact that active isolation mainly targets the low frequency range, the established model can serve the purpose and be easily integrated into any closed-loop control simulations.

(Some figures in this article are in colour only in the electronic version)

1. Introduction

Actuators provide control actions in an active control system. Due to the crucial role they play, there has been a persistent interest in exploring high performance actuators suitable for active control applications. Among a large number of candidates, electromagnetic actuators, hydraulic systems, piezoelectric elements, magnetostrictive actuators and shape memory alloy (SMA) have found applications in noise and vibration control to different extents [1, 2]. Generally speaking, electrodynamic actuators are normally large and heavy for the force they can generate. Hydraulic actuators can provide very high forces but are heavy and limited to low frequencies. Conventional piezoelectric and magnetostrictive actuators can only provide very small displacement. Although SMA actuators are able to generate high displacement, their dynamic response is however limited to a rather low frequency range. Typical vibration control requires an actuator capable of generating sufficient driving force while providing appreciable deformation. The latter is of particular importance in vibration isolation at low frequencies. Due to the aforementioned drawbacks, the exploration for large displacement and force actuators has attracted the attention of many researchers [3–9]. Niezrecki *et al* [3] reviewed some novel concepts used in piezoelectric actuation design to increase the displacement generated by piezoelectric material. The main architectures can generally be categorized into three types: externally leveraged, internally leveraged, and frequency leveraged. Moonie [4], whose name comes from the moon-shaped spaces between the metal end caps and the piezoelectric ceramic, is a typical example of an externally leveraged actuator. Typical examples of internally leveraged actuators include C-blocks [5], Rainbow [6] and THUNDER [7] actuators.

The development of THUNDER actuators (thin layer composite unimorph ferroelectric driver) represents a typical effort made towards this direction. This actuator uses an ultra-high performance hot melt adhesive, LaRC^{TM}-SI, to bond metal foils to PZT ceramic at elevated temperature to create

[1] Author to whom any correspondence should be addressed.

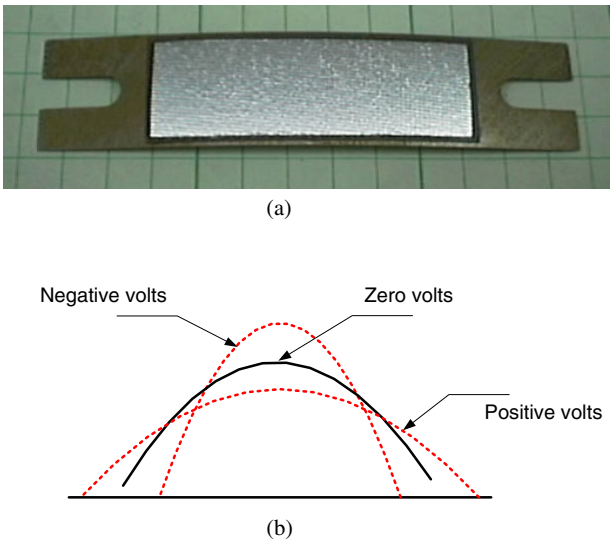

Figure 1. A THUNDER actuator: (a) photo of the actuator; (b) typical deformation under applied voltage.

a pre-stressed condition when cooled to room temperature. The differences in the thermal expansion coefficients of the various bonded layers make up the curved composite laminate as shown in figure 1(a). Thanks to this particular fabrication process, the actuator deforms out of plane as illustrated in figure 1(b), and may generate much larger displacement than conventional piezoelectric actuators with reasonably high loading capacity. In addition to its active property, the curved stainless steel sheet used as the host of the piezoceramics provides a natural flexibility. Therefore, this kind of actuator may be an ideal candidate for the design of an active vibration isolation system, in which both active and passive isolations are needed. This avenue has been explored by two recent papers (Malowicki and Leo [10] and Marouze and Cheng [11]). In the first paper, a THUNDER was characterized and used for active vibration isolation of automotive seats. In the second one, practical issues related to the use of a THUNDER for isolation were discussed. From a different perspective, Jayachandran *et al* [12] used THUNDER actuators as acoustic control sources in the control of low frequency harmonic interior noise.

The aforementioned work showed very promising features of the THUNDER for various active control application. It was also shown that a proper installation of a THUNDER plays a key role in fully exploring its high displacement and loading feature. However, the actual implementation of a THUNDER into a mechanical system is far from simple. The ideal working condition for a THUNDER is to have both ends free, since the vertical displacement at the midpoint of the apex is generated by a change in the radius of curvature. However, practical consideration requires at least one fixed end, which results in a lower displacement in the vertical direction and an undesirable horizontal motion. The latter makes it difficult to physically attach the actuator to mechanical components. It will actually limit the use of THUNDER actuators; therefore a more practical design is essentially required. Another very important issue is the characterization and the modelling of the actuator, which is a crucial element to be integrated in the controller design process. As far as the curved actuators are concerned, various approaches can be considered, e.g. the Thévenin equivalent model [8, 11], the continuum model [13] and the finite element model [14]. The Thévenin equivalent model is simple and effective, but it is not easy to use in simulations because there is no formulation to express the block force and free displacement produced by the actuators. The deformation and force characteristics of a THUNDER can be described through the classical plate and shell continuum theory and finite element method. However, these approaches are complicated and it is difficult to describe the actuator assembly presented in this paper and to be integrated later in simulating the whole control system. It is therefore necessary to develop simple, yet reliable models, describing the electromechanical properties of the actuator.

This paper presents an attempt to tackle these problems. First, an actuator assembly comprising two THUNDERS in a clamshell configuration is designed. The new actuator device conserves the appealing features of the THUNDER and improves its working condition by providing two free edges. A simple model is developed to describe the mechanical and electrical properties of the actuator, on the basis of parameters that can be readily measured experimentally. In order to assess the model, a cantilevered beam connected by one actuator to the base structure is studied both numerically and experimentally. Results show a good agreement between the numerical results and experimental data. The established model can therefore be further used for the design of an active isolation system of other more complex structures.

2. Description of the novel actuator configuration

The THUNDER element used in the actuator assembly is the model TH-8R, which has a physical dimension of 63.5 mm $\times$ 12.70 mm $\times$ 0.483 mm and can generate a maximum displacement of about 2 mm without any loading. The configuration of the new actuator design is shown in figure 2, in which two THUNDER actuators are mounted in a clamshell configuration. Each end of the THUNDER is connected to a V-shaped clip made of flexible stainless steel using small fibre plates as shown in figure 2(b). Two small plastic blocks, attached at the midpoints of the THUNDER apex, are used to connect with the structure for displacement and force transmission. The dimensions of the new actuator are about 12 cm in length and 4 cm height, weighing 15.5 g.

The experiments show that the new actuator assembly can work very well. When an external voltage or loads are applied to the actuator, the two THUNDERs drive the actuator to move back and forth along the axis vertical to the THUNDER apex at the same time. Due to its symmetrical arrangement, both midpoints and ends of the actuator can move freely under the activating voltages or external forces. The passive property of the actuator is not only dependent on the material and structure of the THUNDER, but also on the properties of the steel sheets used in the actuator assembly. Besides the advantages above, the actuator assembly can be inserted and mounted very conveniently between the vibrating structure and the supporting structure like a spring-type element, so overcoming the existing drawbacks in the actual implementation of THUNDER actuators into a vibration or sound isolation system.

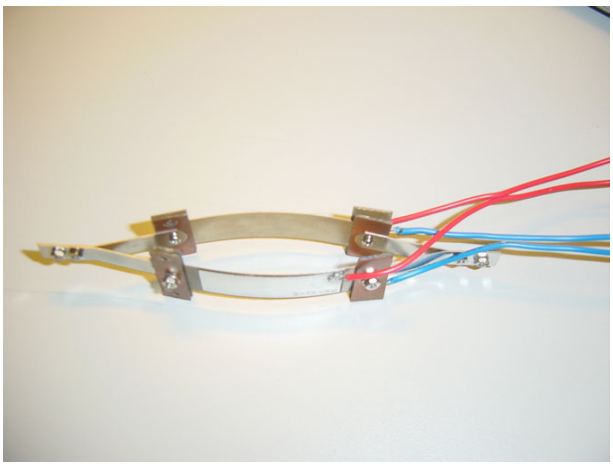

(a)

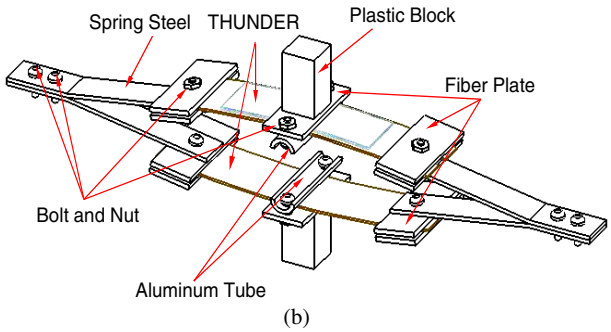

(b)

Figure 2. The proposed actuator assembly: (a) a photograph of the new design; (b) the components of the new design.

3. Characterization of actuators and the measurement of mechanical and electric parameters

3.1. Electromechanical model of the actuator

The actuator assembly presented above exhibits both mechanical and electrical properties at the same time, like other piezoelectric actuators. A complete description of the relationship between the mechanical and electrical parts of the actuator is therefore required. The constitutive equation of piezoelectric material [15] provides a solid basis to establish such a model. Assuming linearity of elasticity and piezoelectricity, the relationship between the mechanical and electrical properties of the new actuator can be expressed by

$$\begin{bmatrix} f \\ I \end{bmatrix} = \begin{bmatrix} K & e_1 \\ e_2 & \Re \end{bmatrix} \begin{bmatrix} \Delta x \\ V \end{bmatrix} \tag{1}$$

where f, x, are, respectively, the force and the displacement along the vertical direction at the apex of the arc as shown in figure 3; I and V are the electrical current and voltage. $K_0 = \frac{f}{\Delta x}|_{V=0}$ is the dynamic stiffness (force per unit displacement) of the actuator with electric circuit open, and $K = K_0(1+\eta j)$, with η being the loss factor. $e_1 = \frac{f}{V}|_{x=0}$ is the force per unit voltage when the actuator is blocked. $e_2 = \frac{I}{\Delta x}|_{V=0}$ is the current per unit displacement with electric circuit open. $\Re = \frac{I}{V}|_{x=0}$ is the electric admittance (current per unit voltage) when the isolator is blocked.

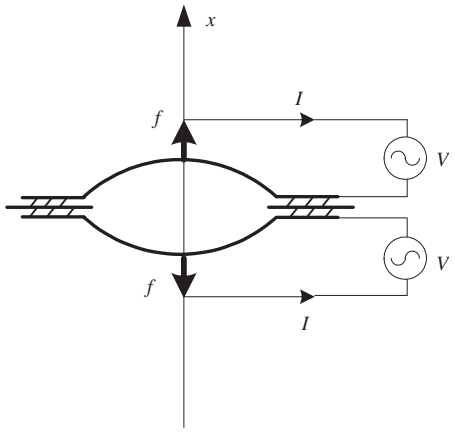

Figure 3. A model of the new actuator.

All four parameters are interrelated. If there is no external load applied to an isolator, i.e. $f = 0$, the free displacement x_f, electric voltage and current will be obtained from equation (1):

$$V = -\frac{K}{e_1}x_f \qquad \text{or} \qquad \frac{x_f}{V} = -\frac{e_1}{K}$$
$$I = \left[e_2 - \frac{K\Re}{e_1}\right]x_f. \tag{2}$$

If the actuator is blocked, i.e. $x = 0$, the blocked force f_b, electric voltage and current from equation (1) will be

$$V = -\frac{f_b}{e_1} \qquad \text{or} \qquad \frac{f_b}{V} = -e_1$$
$$I = \Re V \qquad \text{or} \qquad \frac{I}{V} = \Re. \tag{3}$$

It can be seen that all four parameters in equation (1) can be obtained if the following three groups of parameters can be obtained: $\frac{x_f}{V}$, the free displacement per unit voltage in the absence of any external load. $\frac{f_b}{V}$, the blocked force per unit voltage as the actuator is blocked with zero displacement; and $\frac{I}{V}$, the electric admittance as the actuator is blocked. It is pertinent to note that the first two groups of parameters are frequency dependent, whilst the last one is a constant provided by the manufacturer. The loss factor η can be obtained by a measurement of the time taken for the actuator vibration to decay by 60 dB [16] after cessation of an excitation force,

$$\eta = \frac{4.4\pi}{T_{60}\omega} \tag{4}$$

where T_{60} is the reverberation time in seconds and ω is the frequency of excitation.

3.2. Measurements of mechanical and electrical properties

Various tests were carried out to obtain the parameters used in the aforementioned model. The free displacement x_f was measured by applying a sinusoidal voltage to the actuator in the absence of any external load. The test set-up is shown in figure 4, in which one side of the actuator was attached to a rigid surface. The input voltage signal was amplified by a Piezo Driver/Amplifier (TReK PZD 700) under 1 kHz. A laser

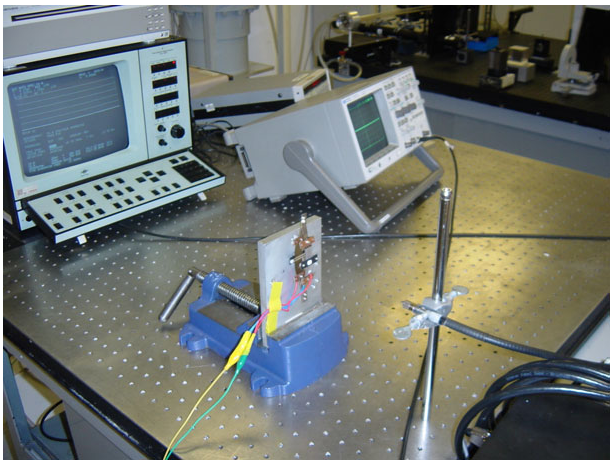

Figure 4. The experimental set-up to measure the free displacement.

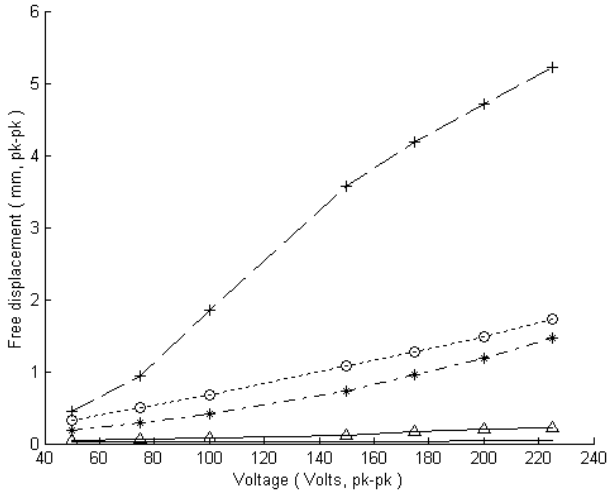

Figure 5. Free displacements versus exciting voltage at different excitation frequencies: 10 Hz - - - - ∗ - - - -; 50 Hz - - - - + - - - -; 60 Hz ——O——; 100 Hz ——△——; and 200 Hz ——.

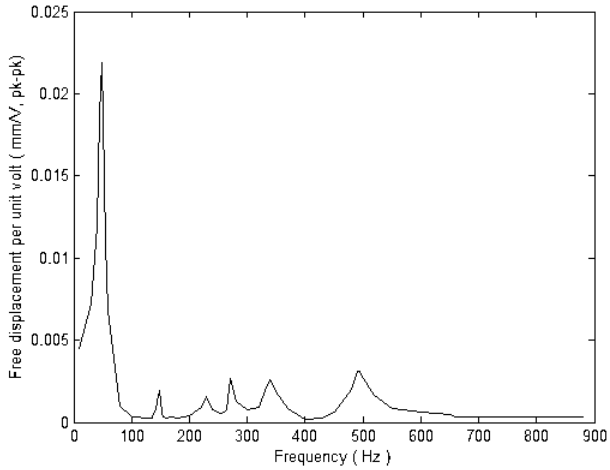

Figure 6. Free displacements per unit volt versus exciting frequency.

vibrometer (Polytech OFV-512/3001) was used to measure the free response of the actuator at the midpoint of apex. Figure 5 shows the measured peak-to-peak values of the free displacements with sinusoidal excitation voltage at different frequencies of 10, 50, 60, 100 and 200 Hz. It can be seen that the relation between free displacements and amplitude of the actuating voltage at most testing frequencies (e.g. 10, 60, 100 and 200 Hz) can be roughly considered to be linear. An exception occurs for 50 Hz, where the actuator experienced a maximum displacement with more apparent nonlinearity appearing. The plausible explanation is that the actuator assembly is a structure itself and may undergo resonances around 50 Hz. This is confirmed by figure 6, which shows the narrow band frequency response of the free displacement per unit voltage of the actuator from 0 to 900 Hz. It can be seen from figure 6 that the structural characteristics of the actuator itself have significant effect on the free displacement per unit voltage. For example, a dominant peak can be observed at 51 Hz, which corresponds to the first natural frequency of the actuator assembly itself. Though less pronounced, higher-order resonances are also noticeable at 150, 224, 278, 354 and 490 Hz. In the low frequency range, where active control is envisaged, the behaviour of the actuator can be roughly approximated by a one degree-of-freedom system.

The blocked force f_b was then measured as the actuator was constrained to prevent any displacement as shown in figure 7. A force transducer (B&K 8200), mounted between the actuator and a rigid beam which blocked the actuator to move vertically, was used to measure the force produced by the actuator. Figure 8 shows the test results of the blocked force versus the exciting voltage at different frequencies: 10, 30, 60, 100 and 200 Hz. It is demonstrated that there exists an approximate linear relation between the blocked force and exciting voltage for the frequencies of 10, 30, 60 and 100 Hz, but at 200 Hz, the blocked force significantly increased with the increase of the exciting voltage. This reveals that the blocked force is also frequency dependent, like the free displacement. This is confirmed by figure 9, which shows the test results of the blocked force per unit voltage with exciting frequencies within 0–900 Hz. This illustrates that the blocked force per unit voltage undergoes strong variations with the actuating frequency above 200 Hz. The maximum blocked force per unit voltage occurs around the frequency of 350 Hz (around the fifth natural frequency of the actuator itself). It is noticed that the maximum blocked forces per unit voltage does not take place around the first natural frequency of the actuator by comparing figure 9 with figure 6, although there is a much larger free displacement at 51 Hz. This means that the structural characteristics of the actuator have a significant effect on the blocked force only when the exciting frequencies are higher (over 200 Hz).

The frequency-dependent characteristics of both the blocked force f_b and the free displacement x_f are considered in numerical simulations presented hereafter. The blocked force per unit voltage is considered to be approximately constant, at about 0.02 N V^{-1} for lower frequencies (0–180 Hz); it increases linearly from 180 to 320 Hz and decreases from 320 to 450 Hz, before becoming constant again at about 0.1 N V^{-1} for frequencies higher than 500 Hz. The dynamic stiffness of the actuator can be obtained from equation (2) using free displacement and blocked force data. Typical values of the

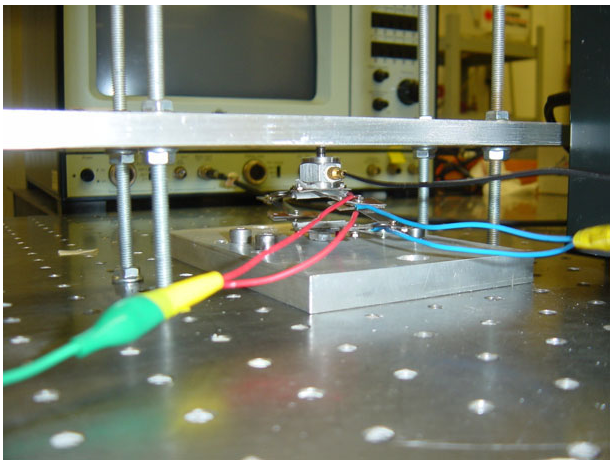

Figure 7. The experimental set-up to measure the blocked force.

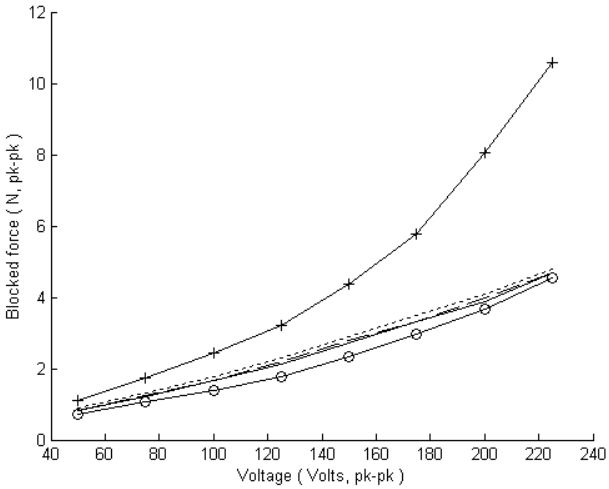

Figure 8. Blocked force versus exciting voltage at different excitation frequencies: 10 Hz ——o——; 30 Hz ——; 60 Hz - - - -; 100 Hz · · · · · ·; and 200 Hz —— + ——.

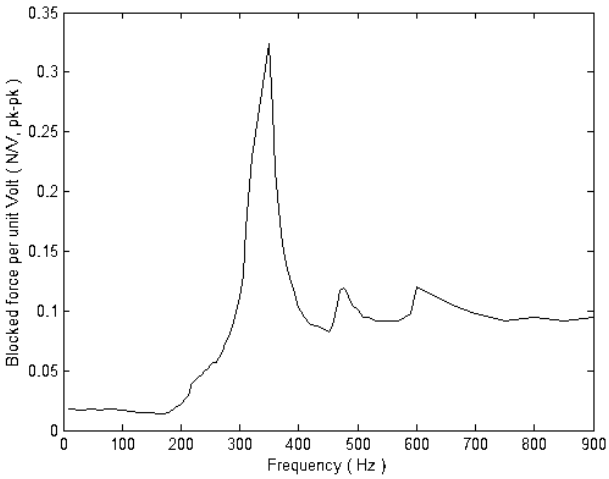

Figure 9. Blocked force per unit voltage versus exciting frequency.

dynamic stiffness are around 10^3 N m^{-1} for lower frequencies (0–180 Hz) and about 10^5 N m^{-1} for the higher frequency range over 600 Hz, while the stiffness without exciting voltage

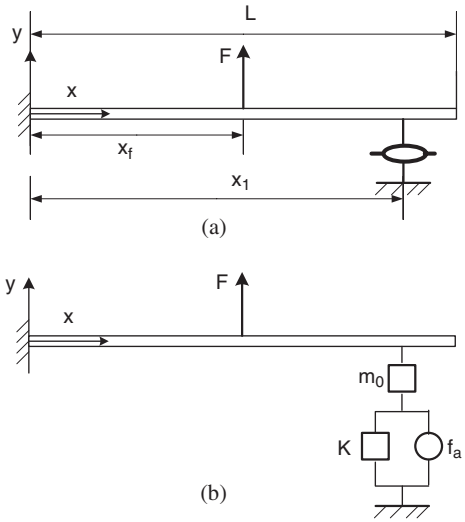

Figure 10. A cantilever beam system with an actuator: (a) the system with a new actuator; (b) a model of the coupled system.

(pure passive case) is 5×10^2 N m^{-1}. The loss factors of the actuator were measured to be about 0.07.

4. The governing motion equations of the coupled system

In order to verify the practicality of the new actuator and the model described in sections 2 and 3, a system including one cantilever beam connected by one actuator to the base structure as shown in figure 10(a) is numerically and experimentally investigated in this section. When there is an external excitation force applied to the beam, the vibration can be controlled by the active effect of the actuator when applying a control voltage to it. In order to obtain more accurate numerical results, the mass of the actuator itself m_0 is included in the simplified model, as shown in figure 10(b). Based on classical beam theory, the governing motion equations of the system can be expressed

$$EJ\frac{\partial^4 y}{\partial x^4} + \rho h\frac{\partial^2 y}{\partial t^2} = F\delta(x - x_f) - f\delta(x - x_1) - m_0\ddot{y}\delta(x - x_1) \tag{5}$$

$$f = Ky + f_a = Ky + eV \tag{6}$$

where y is the transverse displacement of the beam and E, ρ, J are the elastic modulus, mass density and the inertia moment of the beam, respectively. $\delta(x - x_1)$ is the Dirac delta function. $F = F_0 \sin(\omega t)$ is the external harmonic exciting force applied to the beam. f represents the force generated by the actuator and applied to the beam at the connecting point. This force can be divided into two parts: mechanical force and electrical force. K is the dynamic stiffness of the actuator, and $K = K_0(1 + \eta j)$ when the actuator's damping is considered, where η is the loss factor. e, V are the blocked force per unit voltage of the actuator and the control voltage applied to the actuator, respectively.

The transverse displacements of the beam subjected to a harmonic exciting force or voltage can be expressed by the

well known eigenfunction expansion theorem [16].

$$y(x,t) = \sum_{m=1}^{M} A_m \psi_m(x) \sin(\omega t) = [\psi(x)][A]\sin(\omega t)$$
$$[\psi(x)] = [\psi_1(x), \psi_2(x) \cdots \psi_M(x)], \qquad (7)$$
$$[A] = [A_1, A_2 \cdots A_M]^{\mathrm{T}}$$

where ω is the excitation frequency, and $\psi_m(x)$ are the eigenfunctions of the beam which must satisfy all geometric boundary conditions at the edges $x = 0$, $x = L$. For a cantilever beam, the eigenfunctions are as follows:

$$\psi_m(x) = \cos(q_m x) - \cosh(q_m x) + r_m[\sin(q_m x) - \sinh(q_m x)]$$
$$q_1 = \frac{1.875}{a}, \qquad q_2 = \frac{4.214}{a},$$
$$q_m = \frac{(m-0.5)\pi}{a}, \qquad m = 3, 4 \ldots \qquad (8)$$
$$r_m = \frac{\sin(q_m a) - \sinh(q_m a)}{\cos(q_m a) + \cosh(q_m a)}.$$

These characteristic functions used here have the following orthogonal properties:

$$\int_0^L \rho S \psi_m(x)\psi_n(x)\,\mathrm{d}x = \begin{cases} 0 & \text{if } m \neq n \\ \Lambda_m & \text{if } m = n \end{cases} \qquad (9)$$

where S is the cross-sectional area of the beam. The natural frequencies of cantilever beam can be obtained by

$$\omega_m = (q_m L)^2 \sqrt{\frac{EJ}{\rho S L^4}}. \qquad (10)$$

Substituting equations (7) and (6) into (5) and multiplying both sides by $\psi_m(x)$ respectively, then integrating over the length of whole beam on both sides and using the orthogonal properties, equation (5) becomes

$$\begin{aligned}\Lambda_m[\omega_m^2(1 + j\eta_m) - \omega^2]A_m &= \int_0^L [F_0\delta(x - x_{\mathrm{f}}) \\ &\quad - f\delta(x - x_1) + m_0\omega^2 y\delta(x - x_1)]\psi_m(x)\,\mathrm{d}x \\ &= F_0\psi_m(x_{\mathrm{f}}) - f(x_1)\psi_m(x_1) + m_0\omega^2 y(x_1)\psi_m(x_1) \\ &= F_0\psi_m(x_{\mathrm{f}}) + [m_0\omega^2 - K]y(x_1)\psi_m(x_1) - eV\psi_m(x_1) \\ &= F_0\psi_m(x_{\mathrm{f}}) + [m_0\omega^2 - K][\psi(x_1)][A]\psi_m(x_1) - eV\psi_m(x_1)\end{aligned} \qquad (11)$$

which can be expressed in matrix form as

$$\begin{aligned}[M][A] &= F_0[\psi(x_{\mathrm{f}})]^{\mathrm{T}} + [m_0\omega^2 - K] \\ &\quad \times [\psi(x_1)]^{\mathrm{T}}[\psi(x_1)][A] - eV[\psi(x_1)]^{\mathrm{T}}\end{aligned} \qquad (12)$$

where

$$[M] = \begin{bmatrix} \Lambda_1[\omega_1^2(1 + j\eta_1) - \omega^2] & 0 & \cdots & \cdots & 0 \\ 0 & \Lambda_2[\omega_2^2(1 + j\eta_2) - \omega^2] & \cdots & \cdots & 0 \\ 0 & 0 & \cdots & \cdots & 0 \\ \vdots & \vdots & \cdots & \cdots & 0 \\ 0 & 0 & \cdots & \cdots & \Lambda_m[\omega_m^2(1 + j\eta_m) - \omega^2] \end{bmatrix}.$$

Rearranging equation (12) yields

$$\begin{aligned}&\{[M] - [m_0\omega^2 - K][\psi(x_1)]^{\mathrm{T}}[\psi(x_1)]\}[A] \\ &\quad = F_0[\psi(x_{\mathrm{f}})]^{\mathrm{T}} - eV[\psi(x_1)]^{\mathrm{T}}.\end{aligned} \qquad (13)$$

Having obtained the unknowns of $[A]$ from equation (13), the responses of the system can be obtained from equation (7).

By neglecting the excitation force, electrical voltage and loss factors, the natural frequencies of the coupled system can be calculated by solving the eigenvalue problem of the following coefficient matrix:

$$\mathrm{Det}|[M] - [m_0\omega^2 - K][\psi(x_1)]^{\mathrm{T}}[\psi(x_1)]| = 0. \qquad (14)$$

The purpose of the active control being to minimize the resulting flexural vibration level in the beam, the following cost function is adopted [16]:

$$J = \sum_{n=1}^{N} |y_n|^2 \qquad (15)$$

where y_n is the displacement of nth point on the beam. The optimal control voltage can be determined by minimizing the cost function.

5. Theoretical and experimental results and discussions

The cantilever beam shown in figure 10 is made of aluminium with density $\rho = 2700\ \mathrm{kg\,m^{-3}}$, elasticity modulus $E = 7.2 \times 10^{10}\ \mathrm{N\,m^{-2}}$, and Poisson's ratio $\nu = 0.3$. The beam's dimensions are length $L = 0.25$ m, thickness $h = 2$ mm and width $b = 40$ mm. The modal loss factors of the beams are set to be 0.06 for lower modal frequencies and 0.01 for higher modal frequencies. An actuator is connected to the beam on the base structure at $x_1 = 22$ cm. A vertical exciting force is applied at the middle of the beam $x_{\mathrm{f}} = 12.5$ cm. The mass of the actuator itself is $m_0 = 15.5$ g. The natural frequencies of the beam are calculated using equation (10). The first five natural frequencies of the beam itself are 26.7, 134.8, 468.3, 917.9 and 1517.4 Hz. When the mass of the actuator is omitted, the first five natural frequencies of the coupled system obtained by equation (14) are 36.9, 135.1, 468.3, 917.9 and 1517.4 Hz. When the mass of the actuator is considered, the first five natural frequencies of coupled system are 27.7, 132.3, 467.3, 902.5 and 1418.7 Hz. It can be seen that the actuator has a significant influence only on the first modal frequency of the beam if the mass of the actuator is not considered. However, there is an obvious effect on the natural frequencies of the beam, especially for higher modal frequencies, if the mass of the actuator is considered. The calculated results show that the numerical values are accurate enough if the numbers of beam modes are adopted to be $m = 12$.

Experimental tests were carried out using the test set-up illustrated in figure 11. The dimensions and material parameters of the aluminium cantilever beam are the same as in the numerical model shown in figure 10. One end of the beam was clamped on a steel frame, and an actuator was used to connect the beam to the test table. A shaker (B&K Mini Shaker 4810) exerted a driving force on the beam, and the value of the force was measured by a force transducer (B&K 8200). The signal to drive the actuator was

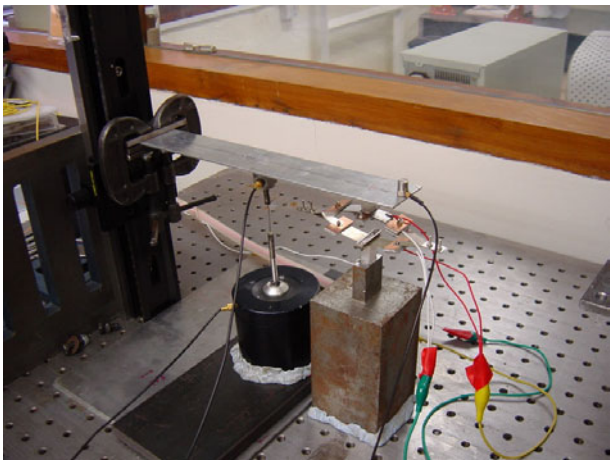

Figure 11. The set-up for passive and active control of a coupled beam.

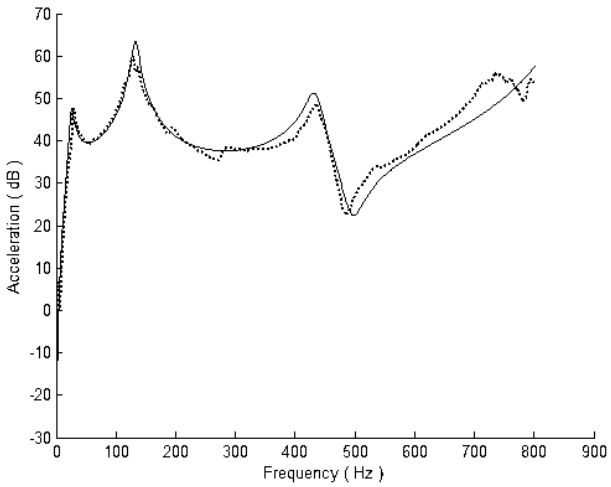

Figure 12. Comparison between the experimental and numerical results of accelerations at the point $x = 25$ cm on the beam (without actuator) excited by a random excitation force at the middle of the beam ($x_f = 12.5$ cm): —— numerical results; · · · · · · experimental results.

amplified by one Piezo Driver/Amplifier (TReK PZD 700). The responses of acceleration or displacement were measured using an accelerometer and a multi-channel signal analyser (B&K type 3550).

First, a single beam without actuator was tested in order to verify the equations and programs. Figure 12 shows the experimental and numerical frequency spectrum responses of vertical acceleration of the beam at the end point ($x = 25$ cm) under random exciting force applied at the middle of the beam ($x_f = 12.5$ cm). Numerical simulations were conducted by letting the stiffness and mass of the actuator be zero in the equations from (11) to (14). It can be seen that the numerical results agree well with experimental results. The series truncation using 12 terms seems to adequately ensure a convergence of the simulation in the whole frequency range considered. This comparison validated the modelling part related to the beam.

Figure 13 shows a comparison between the experimental result and numerical result when considering the passive effect of the actuator only. In this comparison, no external voltage is

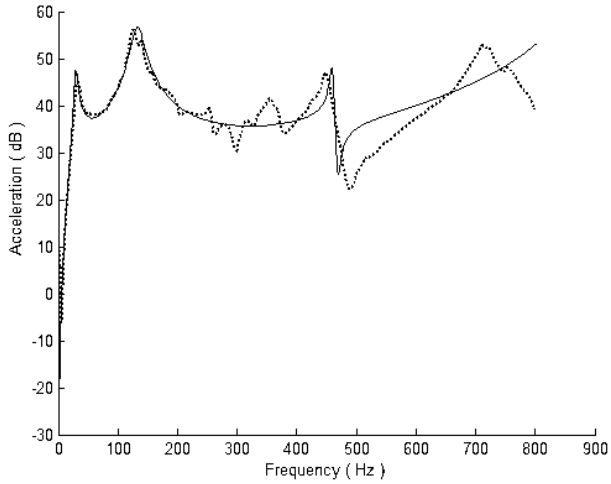

Figure 13. Comparison between experimental and numerical results of the beam excited by a random force without an external control voltage (pure passive case): —— numerical results; · · · · · · experimental results.

provided to the actuator. The accelerations of the end point on the beam ($x = 25$ cm) are plotted, when the beam is excited by a random excitation force at the middle of the beam ($x_f = 12.5$ cm). It can be observed that the experimental and numerical results of the coupled system match very well in the lower frequency range (below 200 Hz). It also displays clearly that the structural characteristics of the actuator have obvious effects on the responses around the natural frequencies of the actuator itself, especially for higher modal frequencies, such as around 224, 278 and 354 Hz. Since the mass of the actuator itself is included in the model as a single freedom spring-supported mass, the actuator dynamics can be characterized very well at lower frequency (before the second modal frequency of the actuator); however, higher-order modes of the actuator cannot be reflected well. Better prediction is certainly possible at the expense of increasing the complexity of the model. It demonstrates that the effect of the actuator itself on the responses of the whole coupled system cannot be neglected when the stiffness and mass of the beam is not large enough compared to the actuator, especially for the higher frequency range where nonlinearity may also occur for the actuator.

A numerical and experimental comparison of the active effect of the actuator is shown in figure 14. In this case, a random external exciting voltage is applied to the actuator with no external force applied. The accelerations of the beam at $x = 25$ cm are used for comparison purposes. In the numerical calculations, different values of the blocked force per unit voltage of the actuator shown in figure 9 were used within different frequency ranges, as spelled out in section 3. It can be seen from figure 14 that the experimental and numerical results match quite well within the range of frequencies 0–150 Hz, and over 500 Hz. Some discrepancies occur, however, in the middle frequency range between 150 and 450 Hz due to the effect of the mass and structural characteristics of the actuator. It can be found again that the characteristics of the actuator itself have a significant effect on the response of the whole system when it is used as an exciter, especially for frequencies around the natural frequencies of the actuator

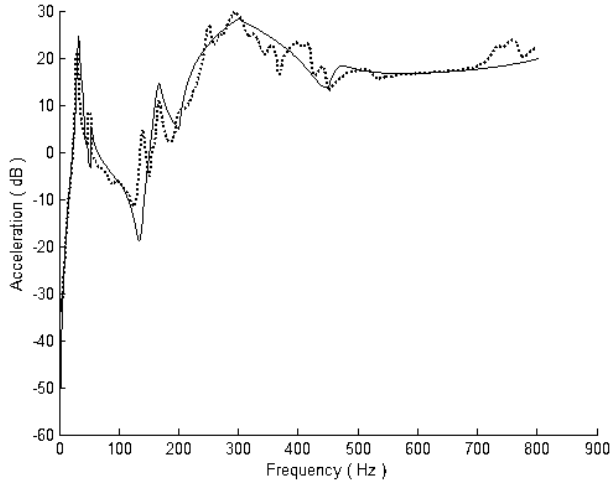

Figure 14. Comparison between experimental and numerical results of the beam excited by external random voltage signals without an external excitation force: —— numerical results; ····· experimental results.

itself. These observations coincide with the facts shown in section 3 that the free displacement and blocked force per unit voltage of the actuator have similar variations with respect to frequency as shown in figures 6 and 9. The model, by including the mass of the actuator itself, can characterize very well the actuator dynamics before and around the first modal frequency of the actuator. It is, however, insufficient to cover the whole frequency range. Fortunately, the THUNDER actuator distinguishes itself from other conventional actuators mainly by its appealing features in the low frequency range. Therefore, potential applications of THUNDERs for active isolation mainly target low frequency, in which the proposed model is of great help.

The verification of the combined passive and active effects of the actuator with the presence of an external excitation force and control voltage at the same time is conducted via two cases. In the first case, the beam is excited simultaneously by a sinusoidal force of 0.1 N (pk–pk) and a sinusoidal control voltage of 20 V with a phase lag of 12.5°, both at 30 Hz. The second case targets a higher frequency of 140 Hz, in which a 0.2 N (pk–pk) force is applied to the beam when the actuator is activated using a 55 V voltage with a phase lag of 22°. In both cases, the forces are applied at the middle of the beam ($x_f = 12.5$ cm), while the acceleration of the beam is examined at its end point ($x = 25$ cm). Since no feedback is involved, the test is apparently open-loop control. Figures 15(a) and (b) show the comparisons between numerical simulations and experiments in time domains for these two cases. In order to facilitate the comparison, passive cases with the actuator inactivated are also included. It can be seen from both figures that the simulations agree well with the test results in both the passive and active cases. With the deployment of the control voltage, the reduction in vibration amplitude of the beam has been accurately predicted by the model.

Experimental results demonstrate that, using the actuator assembly proposed in this paper, vibration can be controlled effectively by the actuator to various degrees within a broad frequency range by adjusting the magnitude and phase of the active control voltage. The vibration can be reduced

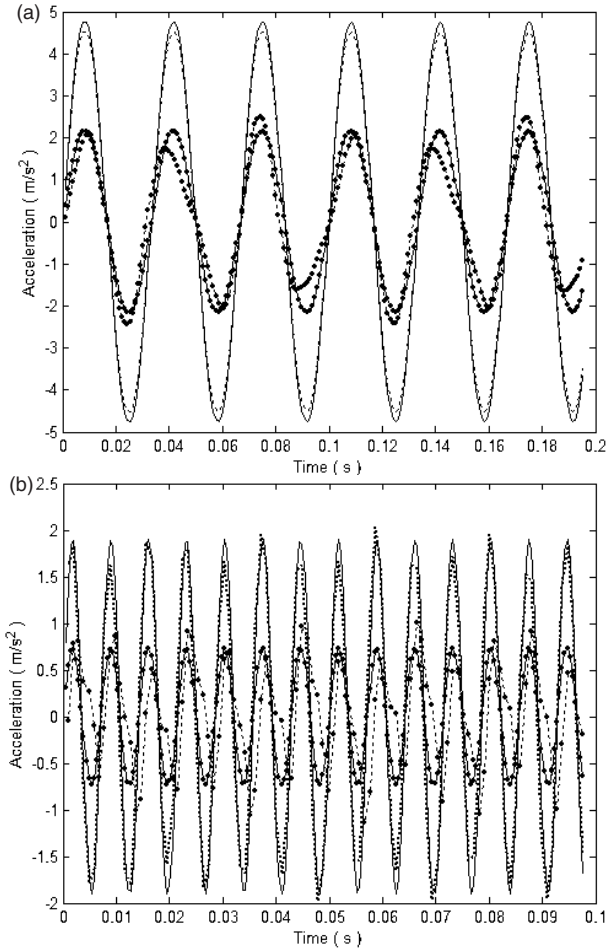

Figure 15. Comparison between experimental and numerical results of accelerations at $x = 25$ cm. (a) With a sinusoidal excitation force of 0.1 N (pk–pk) and a control voltage of 20 V with a 12.5° phase lag at 30 Hz; (b) with an excitation force of 0.2 N (pk–pk) and a control voltage of 55 V with a 22° phase lag at 140 Hz: ····· experimental results for the passive case; – –•– – experimental results for combined active and passive control; —— numerical results for the passive case; ——•—— numerical results for combined active and passive control.

to a minimum when the applied voltage is optimized. The simulation model proposed in the present work can serve this purpose. In fact, by minimizing the cost function defined by equation (15), the optimal control voltage can be determined. An example is given in figure 16, in which the time domain accelerations of the beam are compared using three different control voltages (passive case with $V = 0$; $V = 20$ V and optimal case with $V = 32$ V). It can be seen that the vibration of the beam can be attenuated almost completely when the control voltage is 32 V.

6. Conclusion

A novel actuator configuration is presented in this paper and a model is developed to describe the coupled mechanical and electrical properties of the new actuator assembly. The proposed model is validated using one cantilever beam with one actuator. The modelling of both the passive and active effect of the actuator has been systematically compared with experiments, leading to the following conclusions.

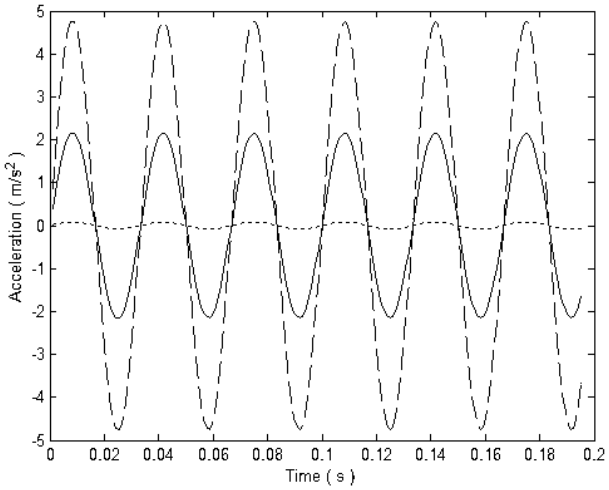

Figure 16. Numerical results of accelerations versus time at $x = 25$ cm on the beam excited by a sinusoidal force of 0.1 N at 30 Hz and controlled by an actuator under different voltages: - - - - $V = 0$; —— $V = 20$ V; $\cdots\cdots$ $V = 32$ V.

The design of the actuator assembly can overcome the existing drawbacks in the installation of THUNDER actuators, while maintaining the passive and active features of the THUNDER. The new actuator can provide larger deformation than one single THUNDER does due to the new configuration, making it an ideal candidate for low frequency active vibration isolation, in which high displacement actuators are usually needed.

The proposed model to describe the new actuator, in which the parameters can be readily obtained by simple tests, can be used effectively in the simulations of the coupled systems. It can provide accurate results below the second natural frequency of the actuator assembly (around 200 Hz in the present case). At higher frequencies, although the model can still correctly predict the overall tendency of the actuator response, an apparent discrepancy has been noticed between simulation and experiments. That is because the dynamics of the actuator has an obvious effect on the response of the whole system near the natural frequencies of the actuator itself. Nevertheless, considering the fact that active isolation mainly targets the low frequency range, the established model can serve the purpose and be easily integrated into any closed-loop control simulations.

Acknowledgment

The work described in this paper was fully supported by a grant from the Research Grants Council of Hong Kong Special Administrative Region, China (Project No PolyU 5155/01E).

References

[1] Brennan M J, Bonito J G, Elliott S J, David A and Pinnington R J 1999 Experiment investigation of different actuator technologies for active vibration control *J. Smart. Mater. Struct.* **8** 145–53

[2] Habibi S and Goldenberg A 1999 A design and analysis of a new symmetric linear actuator for hydraulic and pneumatic system *Trans. Can. Soc. Mech. Eng.* **23** 377–96

[3] Niezrecki C, Brei D, Balakrishnan S and Moskalik A 2001 Piezoelectric actuation: state of the art *Shock Vib. Digest* **33** 269–80

[4] Onitsuka K, Dogan A, Tressler J F, Xu Q, Yoshikawa S and Newnham R E 1995 Metal-ceramic composite transducer, the 'moonie' *J. Intell. Mater. Syst. Struct.* **6** 447–55

[5] Moskalik A J and Brei D 1998 Parametric investigation of the deflection performance of serial piezoelectric C-block actuators *J. Intell. Mater. Syst. Struct.* **9** 223–31

[6] Haertling G H and Robinson G C 1994 Rainbow ceramics—a new type of ultra high displacement actuator *Am. Ceram. Soc. Bull.* **73** 93–6

[7] Copeland B M, Buckley J D, Bryant R G, Fox R L and Hellbaum R F 1999 An ultra-high displacement piezoelectric actuator *NASA Langley Research Center* 23681-0001

[8] Garcia-Bonito J, Brennan M J, Elliott S J, David A and Pinnington R J 1998 A novel high-displacement piezoelectric actuator for active vibration control *J. Smart. Mater. Struct.* **7** 31–42

[9] Yoon K J, Shin S, Park H C and Goo N S 2002 Design and manufacture of a lightweight piezoelectric curved actuators *J. Smart. Mater. Struct.* **11** 163–8

[10] Malowicki M and Leo D J 2001 Active vibration isolation using an induced strain actuator with application to automotive seat suspensions *Shock Vib.* **8** 271–85

[11] Marouze J P and Cheng L 2002 A feasibility study of active vibration isolation using THUNDER actuators *J. Smart. Mater. Struct.* **11** 854–62

[12] Jayachandran V, King P and Meyer N E 1999 Real-time feed-forward control of low-frequency interior noise using shallow spherical shell piezoceramic actuators *J. Smart. Mater. Struct.* **8** 579–84

[13] Hyer M W and Jilani A 1998 A predicting the deformation characteristic of rectangular asymmetrically laminated piezoelectric materials *J. Smart. Mater. Struct.* **7** 784–91

[14] Taleghani B K and Campbell J F 1999 Non-linear finite element modeling of the THUNDER piezoelectric actuators *SPIE Conf. on the Smart Structures and Integrated Systems (Newport Beach, CA)*; *Proc. SPIE* **3668** 555–66

[15] Gao J X and Shen Y P 1998 Three dimensional analysis for vibration of rectangular composite laminates with piezoelectric layers *J. Sound Vib.* **213** 383–90

[16] Hansen C H and Snyder S D 1997 Active control of noise and vibration *(E&FN SPON)*